Applied Catalysis B: Environmental 132–133 (2013) 183–194

Contents lists available at SciVerse ScienceDirect

Applied Catalysis B: Environmental

journal homepage: www.elsevier.com/locate/apcatb

Core–shell Pt modified Pd/C as an active and durable electrocatalyst for the oxygen reduction reaction in PEMFCs

Geng Zhang[a,b], Zhi-Gang Shao[a,*], Wangting Lu[a,b], Feng Xie[a,b], Hui Xiao[a,b], Xiaoping Qin[a], Baolian Yi[a]

[a] Fuel Cell System and Engineering Group, Dalian Institute of Chemical Physics, Chinese Academy of Sciences, 457 Zhongshan Road, Dalian, PR China
[b] Graduate School of Chinese Academy of Sciences, 19A Yuquan Road, Beijing, PR China

ARTICLE INFO

Article history:
Received 14 August 2012
Received in revised form 12 October 2012
Accepted 21 November 2012
Available online 29 November 2012

Keywords:
Proton exchange membrane fuel cell
Oxygen reduction
Electrocatalyst
Core–shell
Platinum
Palladium

ABSTRACT

A series of Pt modified Pd/C catalysts (Pt/Pd/C) with different Pt/Pd molar ratio (Pt:Pd = 1:4, 1:2 and 1:1) are synthesized by a chemical reduction method for oxygen reduction reaction (ORR). X-ray diffraction (XRD), transmission electron microscope (TEM) and cyclic voltammetry (CV) measurements confirm that Pt is deposited on the Pd nanoparticles and the Pt/Pd/C catalysts have a $Pd_{core}@Pt_{shell}$ structure. In the half cell testing, the catalytic ORR activity of $Pt_1/Pd_2/C$ and $Pt_1/Pd_4/C$ are superior to commercial Pt/C. Moreover, the electrochemical durability to potential cycling of $Pt_1/Pd_2/C$ and $Pt_1/Pd_1/C$ catalysts is better than Pt/C catalysts. The improved durability is believed to be associated with the dissolution of Pd and the corresponding structure transformation from core–shell structure to Pt-Pd alloy with Pt rich surface. The structure change is confirmed by TEM, CV, XRD and X-ray photoelectron spectroscopy (XPS). In addition, the electrochemical active surface area (ECSA) loss and polarization behavior in the single cell testing also suggest that the Pt/Pd/C show a much better durability than Pt/C catalysts. Similarly, the dissolution of Pd is observed by CV and scanning electron microscope-energy dispersive X-ray spectra (SEM-EDX). The Pt/Pd/C electrocatalysts have high ORR activity and this high activity can be further improved during potential cycling, that is, the activity and durability can be obtained simultaneously. This $Pd_{core}@Pt_{shell}$ structure allows for the development of highly active and durable ORR electrocatalysts, with potential for the application in proton exchange membrane fuel cells (PEMFCs).

1. Introduction

Proton exchange membrane fuel cells (PEMFCs) are considered to be a promising candidate for the future generation of power solutions for vehicles due to the high power density, high efficiency and low emissions [1]. However, there are many barriers that limits the widespread application of PEMFCs and it is believed that cost and durability are the major two challenges to fuel cell commercialization [2].

A major part of the high cost is attributed to the platinum based electrocatalysts which are usually in the form of nanoparticles dispersed on high surface area carbon support. Due to the inherent slow oxygen reduction kinetics on Pt nanoparticles, the overpotential in fuel cells is attributed in large part to cathode where oxygen reduction reaction (ORR) takes place [3]. Therefore, in order to approach the required power density, the Pt loading on cathode has to be very high which gives rise to the high cost of PEMFCs. In addition, the state-of-the-art Pt/C electrocatalysts will degrade in the cathode due to the high voltage oxidation environment and potential variation conditions like dynamic loading or start-up and shut-up cycles in electronic vehicles. In order to reach the lifetime goal for the PEMFCs used in vehicles, only thicker Pt layers [4] or larger Pt particles [5] can meet this requirement [6]. But these methods will inevitably increase the cost of PEMFCs. Therefore, the activity and durability of ORR catalysts must be improved simultaneously.

It is generally accepted that ORR kinetics on Pt surface is limited by the rate of removal of strongly adsorbed oxygen-containing species (OH_{ad}) [7,8]. Alloying Pt with transition metals (e.g., Cr, Fe, Co, Ni, etc.) was reported to reduce Pt-OH_{ad} formation and to produce some improvements in activity [9,10]. However, a further increase in ORR activity is required to reach the goal of commercialization. Recently, core–shell structured electrocatalysts obtained considerable attention, because the utilization of Pt atoms could be improved and the catalytic ORR activity be greatly enhanced. In addition to the lower price, same FCC crystalline structure and similar atomic size [11], the ORR activity for Pt monolayer on Pd (1 1 1) surface was reported to surpass that of Pt (1 1 1) [12]. Therefore, the Pd core and Pt shell catalysts has received much attention.

Adzic's group developed Pd supported Pt monolayer catalysts ($Pt_{ML}/Pd/C$) via galvanic replacement between Pt and an underpotentially deposited (UPD) Cu monolayer [13]. The Pt mass activity

* Corresponding author. Tel.: +86 411 84379153; fax: +86 411 84379185.
E-mail address: zhgshao@dicp.ac.cn (Z.-G. Shao).

0926-3373/$ – see front matter © 2012 Published by Elsevier B.V.
http://dx.doi.org/10.1016/j.apcatb.2012.11.029

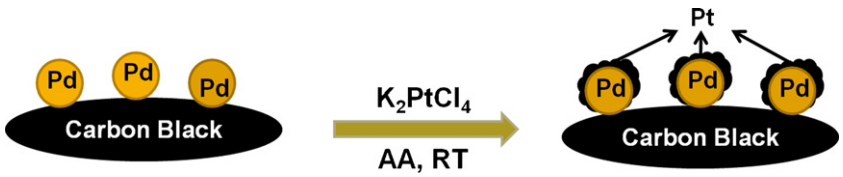

Scheme 1. Synthesis of Pt/Pd/C.

and specific activity of Pt monolayer electrocatalysts is considerably higher than that of commercial Pt/C electrocatalysts due to the weakened Pt-OH_{ad} binding strength and the decrease of the OH_{ad} coverage on the Pt surface caused by the interaction between core and Pt monolayer [8]. And the durability of Pt_{ML}/Pd/C catalysts was evaluated to be much higher than that of Pt/C catalysts in single cell testing, because the core protected the Pt shell by shifting positively its oxidation potential, and by preventing the cathode potential reaching to high values at which Pt dissolution takes place [6]. However, the synthesis method is complicated, and needs special equipments, so it is difficult to make mass production which is required for the application in fuel cells. Xia's group synthesized Pd@Pt core–shell nanostructure by seeded growth method [14,15]. Through the change of reducing agent and reaction conditions, nanodendritic or compact Pd@Pt nanostructures can be prepared. In the synthesis, poly (vinyl pyrrolidone) (PVP) is usually be used as surfactant. However, the interaction between PVP and Pt is so strong that it is hard to completely remove PVP from the Pt surfaces [16]. The remaining PVP will block the active sites of Pt and severely decrease catalytic activity [17]. Recently, the Pd@Pt nanoparticles were prepared by electroless deposition method [18,19]. In this method, Cu is deposited on the surface of Pd by electroless reduction and Pt is deposited on Pd by the galvanic replacement between Pt precursors and Cu. The obtained catalysts presented good ORR activity, but the preparation procedure is complicated, e.g., adjusting pH, consecutive isolation and re-dispersion, and protection of Cu from being oxidized. Besides, the electrochemical durability of the obtained catalysts was not investigated. Based on the summaries above, it can be concluded that Pd_{core}@Pt_{shell} structure is a kind of promising catalysts for PEMFCs. However, in order to meet the practical applications, more efforts should be made at reducing complication of preparation procedure and investigating electrochemical durability under potential cycling conditions.

Here, we made use of commercial 20% Pd/C (BASF) catalysts as substrate and Pt is deposited onto the Pd nanoparticles by a chemical reduction method. The obtained Pt/Pd/C catalysts have a Pd_{core}@Pt_{shell} structure. The Pd@Pt catalysts are prepared by one step without further treatment and the Pd@Pt nanoparticles have uniform dispersion on the carbon black. In the half cell and single cell testing, Pt/Pd/C catalysts exhibit better ORR activity and electrochemical durability than commercial Pt/C catalysts. This enhanced performance results from the dissolution of Pd and the corresponding structure transformation. The preparation method used here is facile and what is more important is that both the activity and durability of Pt/Pd/C catalysts can be improved simultaneously.

2. Experimental

2.1. Synthesis of Pt/Pd/C electrocatalysts

As presented in Scheme 1, Pt was deposited on the Pd/C by the reduction of ascorbic acid (AA). Firstly, Pluronic F127 ($PEO_{106}PPO_{70}PEO_{106}$, Sigma Aldrich) served as surfactant was added to deionized water to give the concentration of 10 mg mL^{-1}. After F127 was completely dissolved, 20% Pd/C (BASF) was dispersed in the above solution with concentration of 2 mg mL^{-1}, and the mixture was vigorously sonicated 30 min before a given amount of 19.1 mM K_2PtCl_4 aqueous solutions was added. Subsequently, 0.4 M AA aqueous solution was added and the mixture was stirred overnight at room temperature. The product was collected by centrifugation, followed by consecutive washing/centrifugation cycles several times with ethanol and water. And then, the obtained product was dried at 60 °C under vacuum overnight. The as-prepared electrocatalysts were denoted as Pt_1/Pd_4/C, Pt_1/Pd_2/C and Pt_1/Pd_1/C for the nominal Pt/Pd molar ratio of 1:4, 1:2 and 1:1, respectively.

2.2. Electrochemical study

Electrochemical study were performed at room temperature on CHI 730D electrochemical station (CH Instruments, Inc.) with a rotating disk electrode system in a conventional three electrode electrochemical system. Electrolyte was chosen to be 0.5 M H_2SO_4 aqueous solutions. Saturated calomel electrode (SCE) and Pt foil was used as reference and counter electrode, respectively. Rotating disk electrode (RDE) with a glassy carbon disk (4 mm in diameter) was used as working electrode. All electrode potentials were given versus reversible hydrogen electrode (RHE). Electrocatalysts slurry was prepared as follows: 5 mg electrocatalysts was dispersed in a 2.5 mL mixture of isopropanol and 5% Nafion solution. The mixture was sonicated for 20–30 min to form an ink, and a given amount of this ink was dropped on the glassy carbon disk and allowed to dry in air at room temperature.

Before electrochemical test the potential of working electrode was scanned between 0.2 and 1.22 V at 100 mV s^{-1} in N_2-purged electrolyte for several times in order to clean the

Table 1
Comparison of Pt/Pd molar ratio before and after half-cell ADT, peak position of 2θ (2 2 0) in XRD profile and peak potential of surface metal oxides reduction peak on CV curves for 20% Pd/C (BASF), 40% Pt/C (JM) and Pt/Pd/C catalysts.

Samples	Pt/Pd molar ratio before half-cell ADT	Pt/Pd molar ratio after half-cell ADT	2θ (2 2 0)[a]	*Por*[b]/V vs. RHE
20% Pd/C	n.a.	n.a.	68.02	0.667
Pt_1/Pd_4/C	20:80	58:42	67.83	0.748
Pt_1/Pd_2/C	34:66	67:33	67.74	0.764
Pt_1/Pd_1/C	52:48	75:25	67.67	0.769
40% Pt/C	n.a.	n.a.	67.52	0.760

[a] XRD data.
[b] Peak potential of surface metal oxides reduction peak on CV curves.

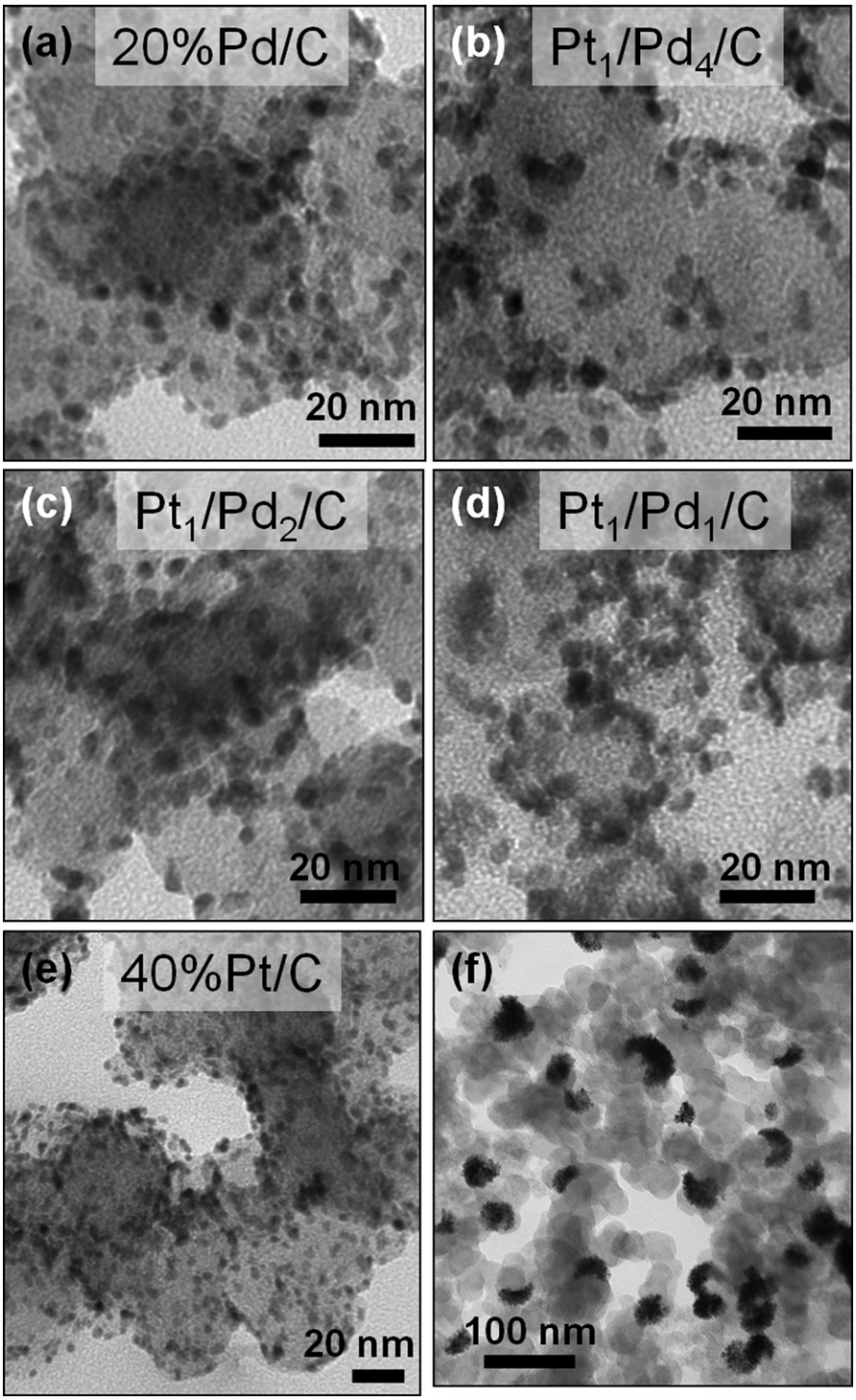

Fig. 1. TEM images of (a) 20% Pd/C (BASF), (b) Pt_1/Pd_4/C, (c) Pt_1/Pd_2/C, (d) Pt_1/Pd_1/C, (e) 40% Pt/C (JM) and (f) Pt nanodendrites/C.

surface of catalysts. The cyclic voltammetry (CV) measurements were carried out in N_2-purged 0.5 M H_2SO_4 solutions at 50 mV s^{-1}. The ORR polarization curves were recorded positively at a sweep rate of 10 mV s^{-1} in O_2-saturated 0.5 M H_2SO_4 at 1600 rpm. The kinetic current of the catalysts is calculated using the well-known mass-transport correction for rotating disk electrodes [10]: $j_k = j_d j/(j_d - j)$, where j is the experimentally obtained current density, j_d is the measured diffusion limiting current density, and j_k the mass-transport free kinetic current density.

The half-cell accelerated degradation test (half-cell ADT) was performed by cycling the potential between 0.62 and 1.22 V at 50 mV s^{-1} in 0.5 M H_2SO_4 under continuous N_2 flow. Cyclic voltammetry curves and ORR polarization curves were measured after half-cell ADT via the method mentioned above.

For comparison, commercial 40 wt.% Pt/C (Johnson Matthey) catalyst was also studied. The specific electrochemical surface area (ECSA) was calculated from integrated hydrogen desorption area in cyclic voltammograms using 0.21 mC cm_{Pt}^{-2} as the conversion factor.

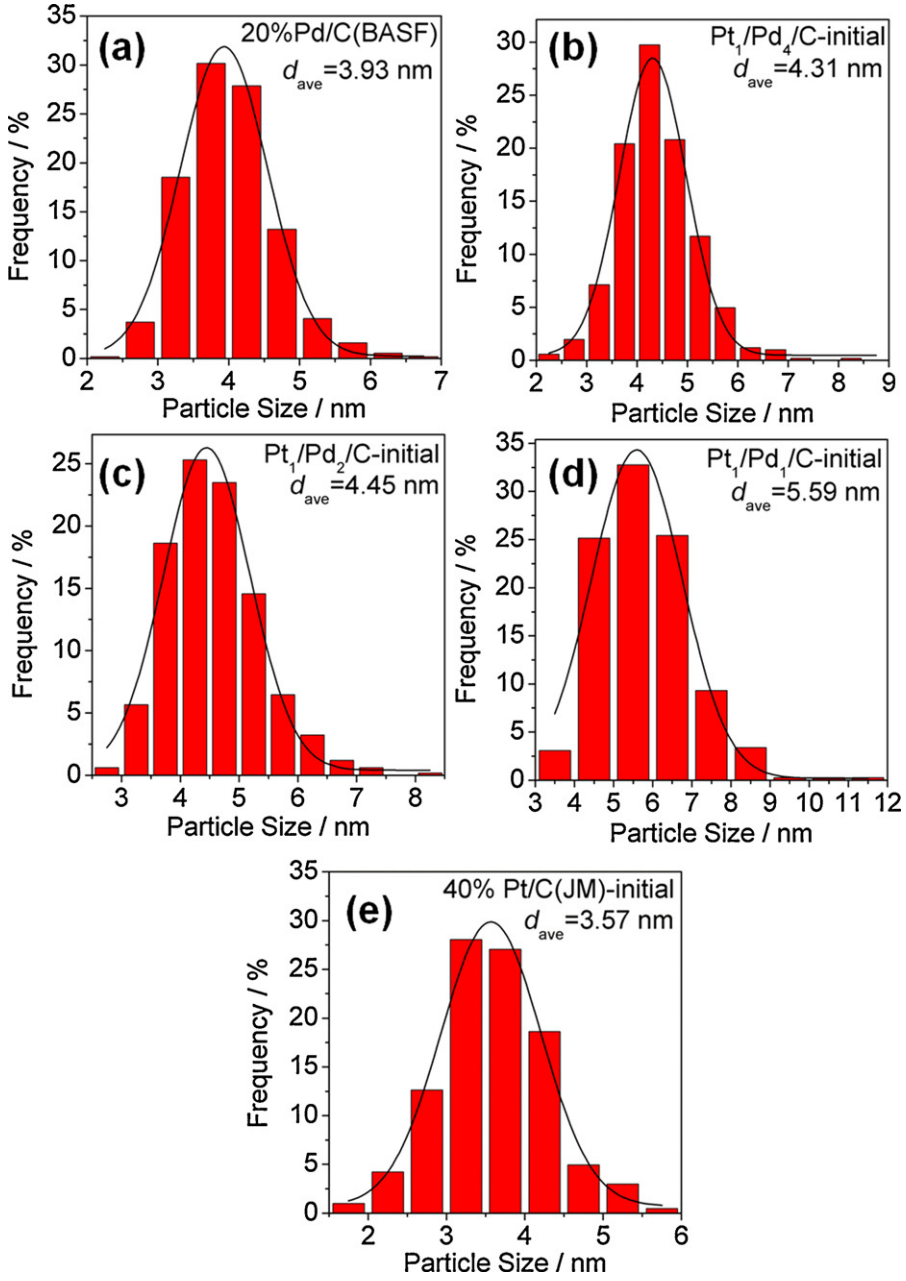

Fig. 2. Particle size distribution for (a) 20% Pd/C (BASF), (b) Pt_1/Pd_4/C, (c) Pt_1/Pd_2/C, (d) Pt_1/Pd_1/C and (e) 40% Pt/C (JM).

2.3. Membrane electrode assembly (MEA) preparation

Commercially available gas diffusion electrode (GDE, Sunrise Power Corp., China) with Pt loading of 0.4 mg_{Pt} cm^{-2} was used as the anode for all fuel cell experiments. The cathode catalyst ink was prepared by ultrasonically blending 40% Pt/C (JM) or Pt/Pd/C electrocatalysts powder with Nafion solution (5 wt.%, Du Pont Corp.) and ethanol for 1 h at an ionomer/carbon weight ratio of 0.7/1. The catalyst ink was then sprayed onto a wet-proofed carbon gas diffusion layer (GDL). The true Pt loading was measured by inductively coupled plasma-atomic emission spectroscopy (ICP-AES) using Perkin Elmer Optima 2000 DV. The MEAs with an active area of 5 cm^2 were fabricated by hot-pressing the anode and cathode electrodes on both sides of a Nafion 212 membrane (Du Pont Corp.) at 140 °C. The MEA was then cooled and assembled in 5 cm^2 single cells for testing.

2.4. Single cell testing

The single cell was conditioned with fully humidified H_2 and O_2 under 65 °C and 150 kPa_{abs} at 500 mA cm^{-2} overnight and at 1000 mA cm^{-2} for at least 4 h before polarization curves were recorded. Both the polarization curves and the internal resistance of the fuel cell (at 10 kHz) were measured by Kikusui KFM-2030 FC Impedance Meter at the same time. After that, the cathode gas was switched to dry N_2 and the cell was cooled down to 30 °C. The cyclic voltammetry (CV) curves were recorded on CHI-600C (CH Instruments, Inc.) with anode as the count and reference electrode (dynamic hydrogen electrode, DHE), and the cathode was cycled between 0 and 1.0 V (vs. DHE) at a sweep rate of 20 mV s^{-1}, using fully humidified H_2 at the anode and dry N_2 at the cathode. The region corresponding to hydrogen desorption region was used to measure the ECSA of the cathode. And then, the cathode gas was

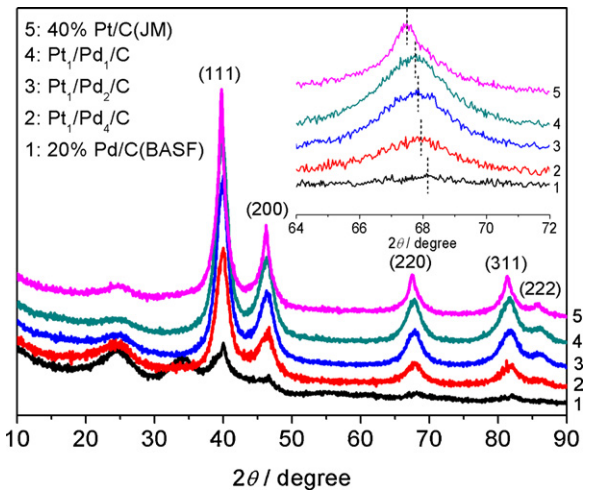

Fig. 3. XRD patterns of 20% Pd/C (BASF), 40% Pt/C (JM), $Pt_1/Pd_1/C$, $Pt_1/Pd_2/C$ and $Pt_1/Pd_4/C$; the insert shows the detailed lines of FCC (2 2 0) peaks.

switched to humidified N_2 and the cell temperature was heated back to 65 °C.

The durability of the cathode electrocatalysts was evaluated using a single-cell accelerated degradation test (single-cell ADT) method. The single-cell ADT was conducted by cycling the cathode potential between 0.65 and 1.05 V (vs. DHE) at a sweep rate of 100 mV s^{-1} at 65 °C. During potential cycling, the cell was fed with humidified H_2 (150 kPa_{abs}) at the anode and N_2 (150 kPa_{abs}) at the cathode. The polarization curve and CV curve were measured after every 10,000 potential cycles.

2.5. Physical characterization

X-ray diffraction (XRD) analysis was conducted on PANalytical X'Pert-Pro powder X-ray diffractometer using Cu Kα radiation (λ = 0.154056 nm). X-ray photoelectron spectra (XPS) were obtained from an ESCALAB 250Xi (Thermo Scientific) spectrometer using Al Kα radiation. Transmission electron microscopy (TEM) images were taken using JEOL JEM-2000EX electron microscope operating at 120 kV. The composition of as-prepared Pt/Pd/C was determined by Oxford Inca EDX detector equipped on JEOL JSM-6360LV scanning electron microscope (SEM), while the composition of Pt/Pd/C after half-cell ADT was measured by inductively coupled plasma atomic emission spectroscopy (ICP-AES, Perkin Elmer Optima 2000 DV). The cross section of the pristine and aged MEAs was obtained by breaking the MEAs in liquid nitrogen. The morphology and elemental distribution of the cross-sectional MEAs were detected by FEI Quanta 450 microscope equipped with Oxford Inca EDX detector.

3. Results and discussion

3.1. Catalysts characterization

The synthesis of Pt/Pd/C was carried out in aqueous solutions at room temperature. As shown in Table 1, the Pt/Pd molar ratio measured by EDX is very close to the nominal value, i.e., all $PtCl_4^{2-}$ was reduced, indicating the efficiency of the synthesis method.

Fig. 1 shows the TEM images of Pd/C and Pt/Pd/C with different Pt/Pd molar ratios. As shown in Fig. 1, all Pt/Pd/C catalysts have spherical particles which are similar to that of Pd/C catalysts. The dispersion of metal particles of $Pt_1/Pd_4/C$ and $Pt_1/Pd_2/C$ on carbon black is better than that of $Pt_1/Pd_1/C$ whose particles are too close with each other. The particle size distributions of catalysts presented in Fig. 2 show that the average particle size of Pt/Pd/C increases with the increase of Pt fraction, from 3.93 nm for Pd/C to 5.59 nm for $Pt_1/Pd_1/C$. Thus the Pt shell thickness is 0.19, 0.26 and 1.66 nm for $Pt_1/Pd_4/C$, $Pt_1/Pd_2/C$ and $Pt_1/Pd_1/C$, respectively. In order to study the effect of Pd nanoparticles in the preparation of Pt/Pd/C, Pd/C was replaced by XC-72R carbon black and the other conditions were remained the same as that of the preparation of $Pt_1/Pd_2/C$. As shown in Fig. 1(f), Pt nanodendrites with diameter at around 20 nm were obtained on XC-72R carbon black, which is obviously different from that of Pt/Pd/C. In the presence of Pd nanoparticles, since the lattice parameter of Pd is very close to that of Pt and ascorbic acid is a relevant mild reducing agent toward K_2PtCl_4 [20], Pt is prone to seed and grow on Pd nanoparticles instead of on the carbon black. From the above, we considered that the Pt/Pd/C catalysts have a $Pd_{core}@Pt_{shell}$ structure.

Fig. 3 shows the XRD patterns of 20% Pd/C, $Pt_1/Pd_4/C$, $Pt_1/Pd_2/C$, $Pt_1/Pd_1/C$ and 40% Pt/C. The diffraction peak at around 25° comes from the carbon black, while the diffraction peaks of the five catalysts at around 40°, 47°, 68°, 81° and 86° are attributed to the (1 1 1), (2 0 0), (2 2 0), (3 1 1) and (2 2 2) planes of the FCC structure of Pt and Pd, respectively. Because Pt and Pd have the same crystal structure (FCC) and very close lattice parameter, the sets of diffraction peaks of Pt and Pd are overlapped [21]. The diffraction peaks of Pt/Pd/C are

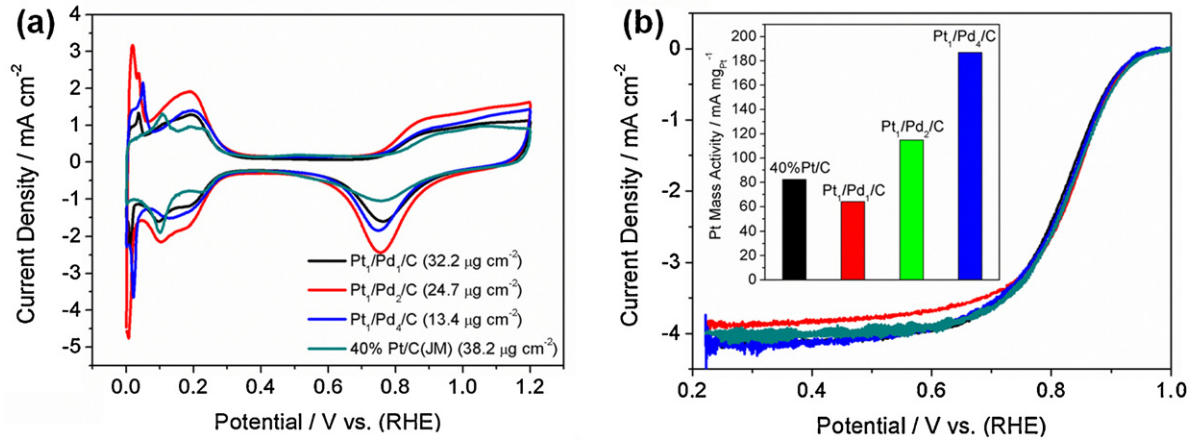

Fig. 4. (a) CV and (b) ORR polarization curves of 40% Pt/C (JM) and Pt/Pd/C in 0.5 M H_2SO_4; the inset of (b) is the comparison of Pt mass activity at 0.85 V (vs. RHE) for these catalysts. The Pt loading of these catalysts on RDE is given in the legend.

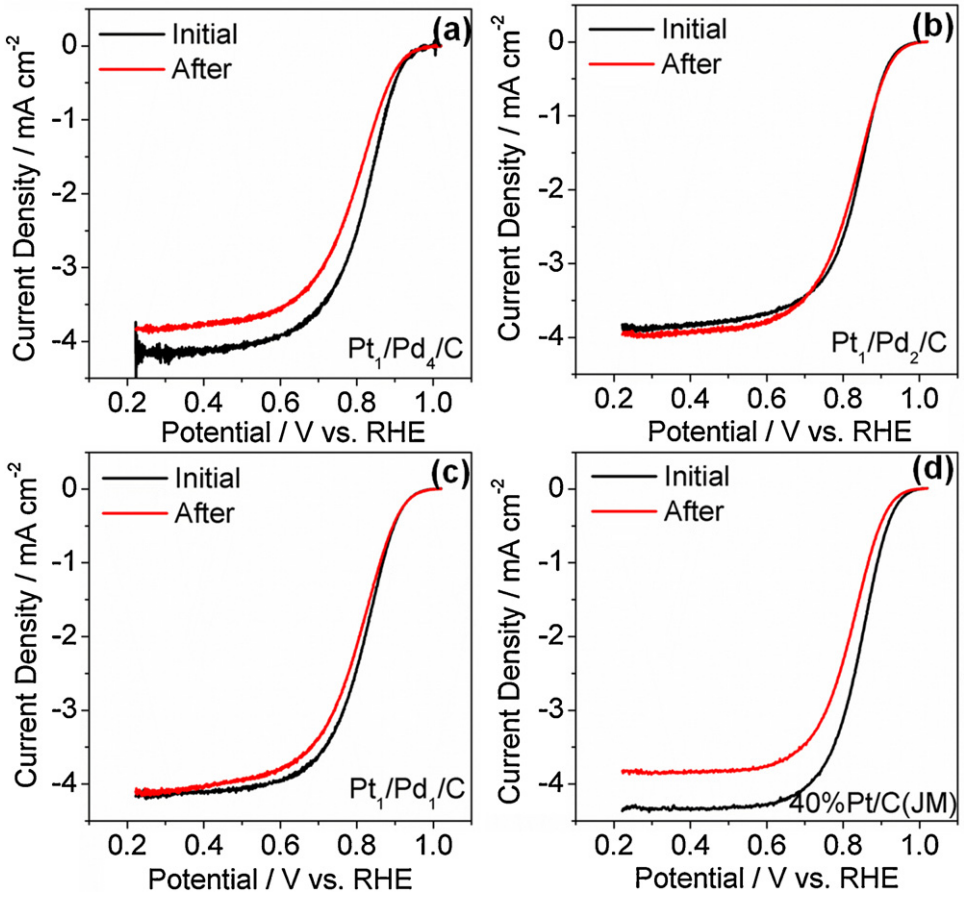

Fig. 5. ORR polarization curves for (a) $Pt_1/Pd_4/C$, (b) $Pt_1/Pd_2/C$, (c) $Pt_1/Pd_1/C$ and (d) 40% Pt/C (JM) before and after half-cell ADT.

remarkably strengthened in comparison to Pd/C, indicating good crystallinity of the Pt/Pd/C catalysts. Furthermore, we observed that the peaks of Pt/Pd/C locate between that of Pd/C and Pt/C (e.g., see (2 2 0) peaks shown in the inset of Fig. 3), which is consistent with the results of core–shell structured nanoparticles reported in literature where the diffraction peaks of core–shell structure locate between the individual core and shell metals [22,23]. In addition, the peak potential of the FCC (2 2 0) peaks decreases in the order of Pd/C > $Pt_1/Pd_4/C$ > $Pt_1/Pd_2/C$ > $Pt_1/Pd_1/C$ > Pt/C (see Table 1), which is consistent with the change of mass fraction of Pt in the catalysts.

As a surface sensitive characterization method, cyclic voltammetry was used to study the surface of electrocatalysts. As shown in Fig. 4(a), the intense peak at about 0.05 V in the hydrogen under potential deposition (H_{upd}) region (0–0.4 V) originates from the Pd surface uncovered by the Pt shell. The curve profile of the H_{upd} region and surface oxidation/reduction region (> 0.6 V) for Pt/Pd/C are different from that of Pd/C (Fig. S1 in Supplementary Materials). In addition, with the increase of Pt/Pd molar ratio, the surface oxides reduction peak shifts positively (see Table 1), indicating that the Pt covering degree increases and the Pd surface exposed is reduced. On the basis of the results of TEM, XRD and CV, we can conclude that the Pt/Pd/C catalysts have a $Pd_{core}@Pt_{shell}$ structure.

3.2. Electrochemical activity and durability in half-cell testing

The polarization curves for ORR were conducted in O_2-saturated 0.5 M H_2SO_4, and after mass-transport correction, the Pt mass activity for Pt/C and Pt/Pd/C was presented in Fig. 4(b). For Pt/Pd/C catalysts with Pt/Pd molar ratio of 1:2 and 1:4, the Pt mass activity is enhanced in comparison with the commercial 40% Pt/C catalysts. The enhancement of catalytic activity of Pt/Pd/C could be attributed to the interaction between Pd core and Pt shell. As already be observed by other researchers [8,12,18], the Pd core will induce compressive strain on the Pt shell, and this compressive strain will reduce the adsorption strength for the adsorbed hydroxyl species on the Pt surface which is supposed to be a block to the oxygen reduction reaction [7,8,12,24,25]. Owing to the thinnest Pt shell, $Pt_1/Pd_4/C$ has the highest mass activity, followed by $Pt_1/Pd_2/C$. With the increase of Pt fraction, the Pt shell will grow thicker, resulting in weakened interaction between the core and shell, which leads to the reduced Pt mass activity of $Pt_1/Pd_1/C$.

The half-cell ADT of catalysts was evaluated by potential cycling between 0.62 and 1.22 V at a sweep rate of 50 mV s^{-1} in N_2-purged 0.5 M H_2SO_4. The number of cycles was limited to 600 cycles so as to avoid the occasional flaking of catalyst particles from the electrode tip when the test time is longer [26]. Additionally, due to the high maximum potential limit (1.22 V) and the fact that sulfuric acid can accelerate the dissolution of metal through the formation of complexes [26], 600 potential cycles were enough to observe the degradation of the electrocatalysts.

The ORR polarization curves for Pt/Pd/C and 40% Pt/C (JM) before and after half-cell ADT are shown in Fig. 5. After 600 potential cycles, the kinetic current density at 0.85 V ($j_{k@0.85\,V}$) for $Pt_1/Pd_1/C$ and $Pt_1/Pd_2/C$ nearly does not decline, while the retention percentage for 40% Pt/C(JM) and $Pt_1/Pd_4/C$ is 54.3% and 59.9%, respectively. The degradation of Pt/C may result from the decrease of ECSA, because only 53.5% of the initial ECSA is remained after half-cell ADT (Fig. S2 (d) in Supplementary Materials). As for Pt/Pd/C catalysts, the CV changed significantly after half-cell ADT, that is, the intense peak at ~0.05 V originating from the Pd surface uncovered by the Pt shell

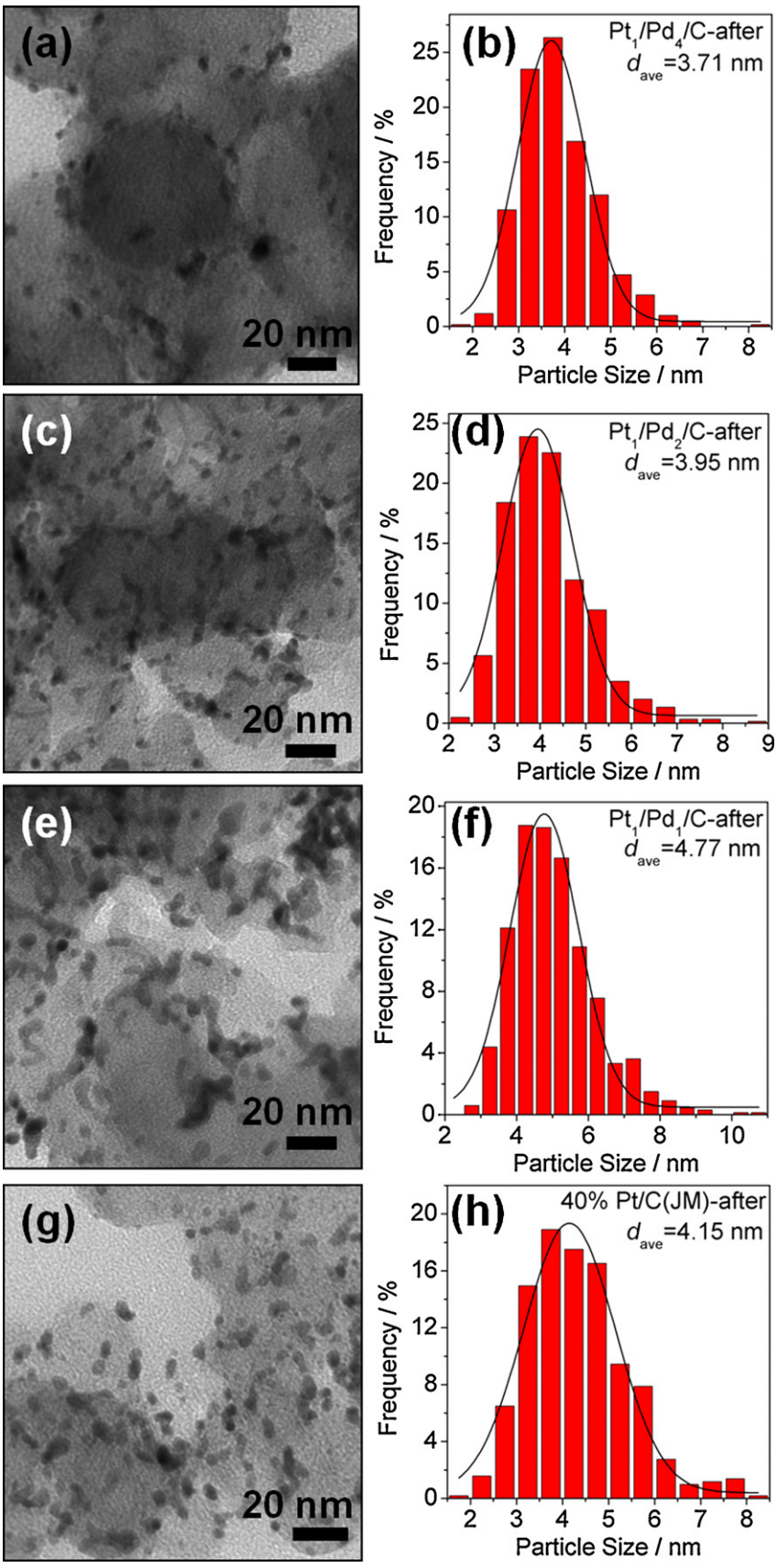

Fig. 6. TEM images and particle size distribution for (a and b) $Pt_1/Pd_4/C$, (c and d) $Pt_1/Pd_2/C$, (e and f) $Pt_1/Pd_1/C$ and (g and h) 40% Pt/C (JM) after half-cell ADT.

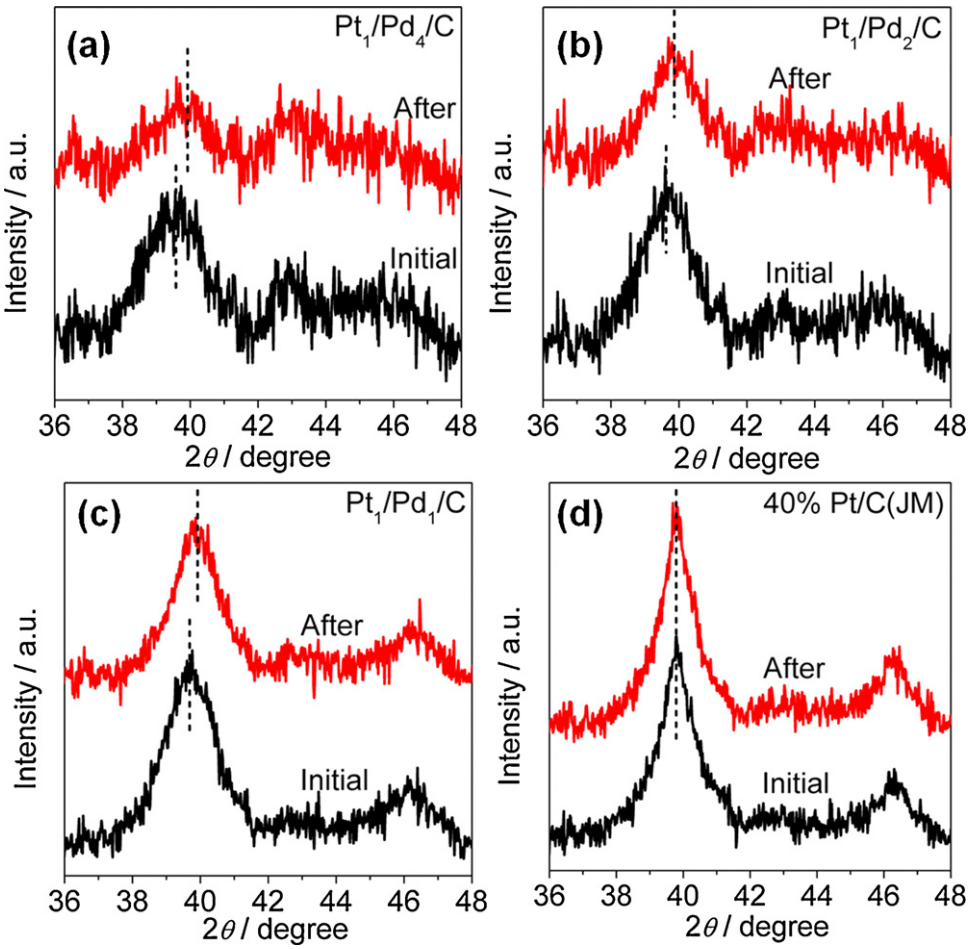

Fig. 7. XRD patterns of (a) $Pt_1/Pd_4/C$, (b) $Pt_1/Pd_2/C$, (c) $Pt_1/Pd_1/C$ and (d) 40% Pt/C (JM) before and after half-cell ADT. All of the catalysts were dropped onto the GDL.

completely disappeared (see Fig. S2 in Supplementary Materials). This result suggests that the Pd core may be dissolved, because the Pd core is not entirely covered by Pt, and the high limit of potential cycling (1.22 V) is higher than the standard electrochemical potential for direct Pd dissolution [0.92 V ($Pd \rightarrow Pd^{2+} + 2e^-$, $U_0 = 0.92$ V)] [27]. In fact, the Pd in Pt/Pd/C catalysts is really diminished after half-cell ADT as shown in Table 1, confirming the dissolution of Pd.

Additionally, the TEM images of Pt/C and Pt/Pd/C catalysts after half-cell ADT and the corresponding particle size distribution are shown in Fig. 6. Compared with Fig. 1, the average particle size of $Pt_1/Pd_4/C$, $Pt_1/Pd_2/C$ and $Pt_1/Pd_1/C$ is decreased after half-cell ADT, which is consistent with the dissolution of Pd core. Specifically, the particle density on carbon black of the aged $Pt_1/Pd_4/C$ is obviously reduced in comparison with the as-prepared samples, because the Pt coverage on Pd is smallest and the dissolution of Pd

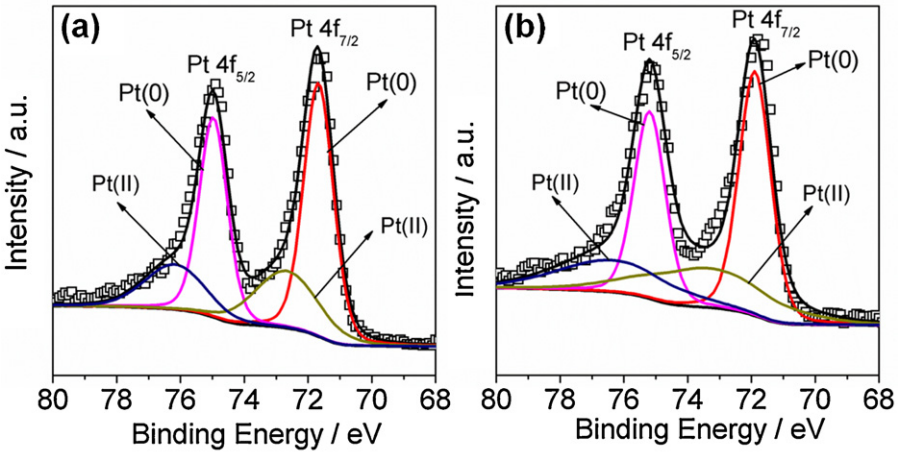

Fig. 8. XPS spectra for Pt 4f region of $Pt_1/Pd_2/C$ (a) before and (b) after half-cell ADT.

Table 2
Atomic ratio, chemical state and binding energy of Pt 4f for $Pt_1/Pd_2/C$ by XPS before and after half-cell ADT.

Catalyst	Atomic ratio of Pt:Pd	Chemical state	Binding energy of Pt $4f_{7/2}$ (eV)	Binding energy of Pt $4f_{5/2}$ (eV)	Relative intensity (%)
Before	51:49	Pt(0)	71.67	74.97	67.7
		Pt(II)	72.67	76.17	32.3
After	81:19	Pt(0)	71.89	75.19	61.9
		Pt(II)	73.34	76.29	38.1

for $Pt_1/Pd_4/C$ is the most significant (see Table 1), leading to the corresponding loss of Pt deposited on Pd nanoparticles. That may give rise to the poor durability of $Pt_1/Pd_4/C$ (Fig. 5(a)). For $Pt_1/Pd_2/C$, the particle density on carbon black appears not to decrease after 600 potential cycles and the particle distribution is uniform. As for $Pt_1/Pd_1/C$, the particle agglomeration is obvious due to the small distance among particles. In contrast, the average particle size of Pt/C increases from 3.57 to 4.15 nm caused by the coalescence and Ostwald ripening, which leads to the degradation of ECSA and ORR activity. It should be pointed out that the decline of limiting current density of $Pt_1/Pd_4/C$ and Pt/C after half-cell ADT may be resulted from the significant decrease of ECSA and specific activity [14,28].

In order to further observe the structure change after potential cycling, the catalyst slurries were casted onto GDL followed by half-cell ADT. The catalyzed GDL were taken XRD and XPS measurements before and after half-cell ADT. The XRD spectra (part) of catalysts before and after half-cell ADT are shown in Fig. 7. Since Pd of Pt/Pd/C was remarkably lost after half-cell ADT, the diffraction peak should have shifted negatively owing to the larger lattice constant of Pt. On the contrary, the (1 1 1) diffraction peaks for Pt/Pd/C catalysts with different Pt/Pd molar ratios all shifted positively after ADT, while the (1 1 1) peak for Pt/C does not change. As observed in the literature, the XRD diffraction peaks for the bimetallic alloyed catalysts will shift positively in comparison with the corresponding core–shell structures whose shell metal has larger lattice parameter than that of the core metal, e.g., Co-Pd [29] and Co-Pt [30] systems. Therefore, on the basis of CV and XRD, we considered that the Pt/Pd/C catalysts were transformed into Pt-Pd alloyed catalysts after half-cell ADT.

Fig. 8(a) and (b) shows XPS spectra in Pt 4f region for $Pt_1/Pd_2/C$ before and after half-cell ADT, respectively, with Table 2 summarizing the peak deconvolution results. For $Pt_1/Pd_2/C$, the peaks at 71.67 and 74.97 eV are assigned to Pt (0) $4f_{5/2}$ and Pt (0) $4f_{7/2}$, respectively. The second and weaker doublet (at 72.67 and 76.17 eV) could be assigned to oxidized Pt species, because catalysts are exposed to air. The Pt/Pd molar ratio of the as-prepared $Pt_1/Pd_2/C$ from XPS analysis is 51:49, indicating Pt enrichment on the outer layer. Since the typical mean free path for photoelectrons in metals is in the range of 1–2 nm and the Pt thickness for $Pt_1/Pd_2/C$ is 0.26 nm, the Pd core could also be detected. After half-cell ADT, the Pt 4f region could be deconvoluted into 71.89 and 75.19 eV for metallic Pt and 73.34 and 76.29 eV for the Pt oxides. The Pt/Pd molar ratio of the aged $Pt_1/Pd_2/C$ is 81:19, which is larger than the bulk Pt/Pd

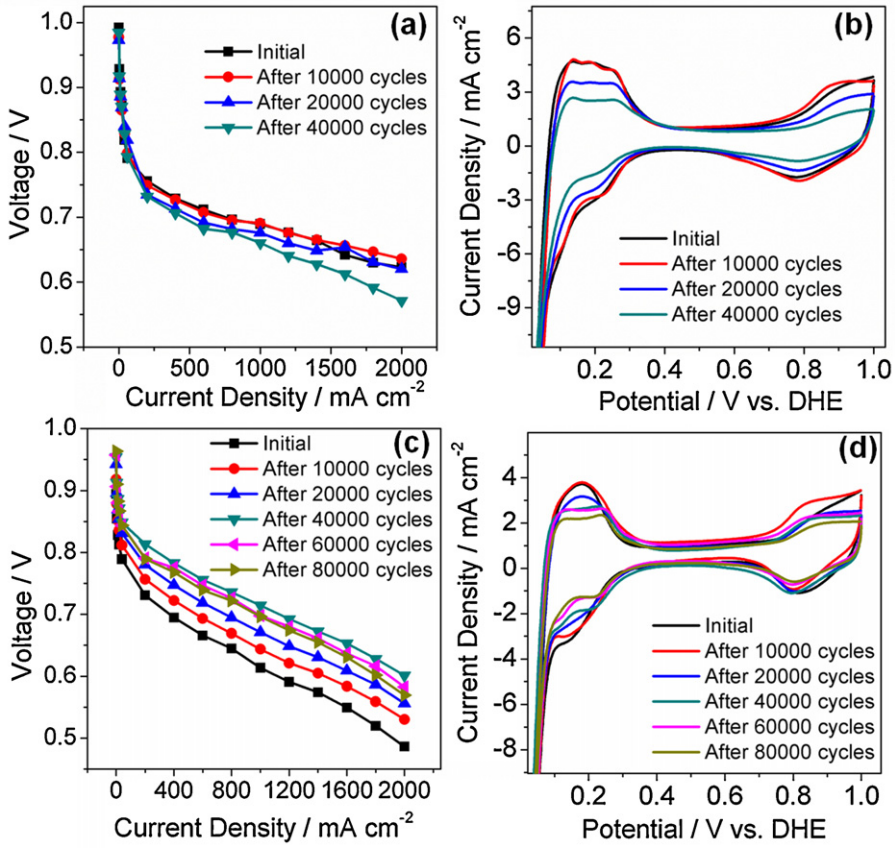

Fig. 9. The IR-corrected polarization and CV curves for the fuel cells with cathodes made by (a and b) 40% Pt/C (JM) and (c and d) $Pt_1/Pd_2/C$ catalysts after different potential cycles between 0.65 and 1.05 V (vs. DHE) with a sweep rate of 100 mV s^{-1} at 65 °C.

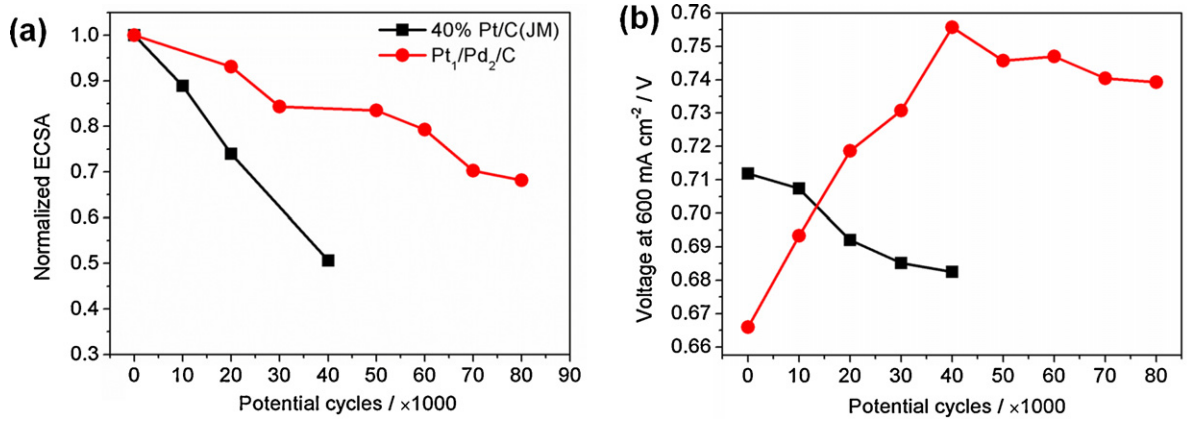

Fig. 10. (a) Normalized ECSA and (b) IR-corrected cell voltage at 600 mA cm^{-2} of fuel cells with cathodes made by 40% Pt/C (JM) and $Pt_1/Pd_2/C$ catalysts as a function of potential cycles between 0.65 and 1.05 V (vs. DHE) with a sweep rate of 100 mV s^{-1} at 65 °C.

molar ratio (67:33), indicating the Pt-Pd alloy obtained has a Pt rich surface and Pd rich core. In addition, it is important to note that the Pt 4f signals of the aged $Pt_1/Pd_2/C$ have shifted positively by 0.22 eV relative to the as-prepared catalysts. The shift can be ascribed to the more remarkable interaction between Pt and Pd [31] and the larger compressive strain induced by the Pd rich core relative to the initial core–shell structure [32], because the interface between core and shell was no longer clear in the Pt-Pd alloy. Similar results have also been observed by other researchers [32,33]. The lattice contraction in the Pt shell will weaken the surface oxygen binding energy, which enhances the ORR specific activity [7,8]. That may explain the better durability of $Pt_1/Pd_1/C$ and $Pt_1/Pd_2/C$ catalysts. On the basis of the above results, we can conclude that it is the dissolution of Pd and the corresponding structure transformation that lead to the better durability of Pt/Pd/C catalysts. On the other hand, the presence of Pt can slow down the dissolution rate of Pd. For the pure Pd/C catalysts, the Pd nanoparticles will completely lose after 100 potential cycles between 0.02 and 1.22 V (see Fig. S1 in Supplementary Materials). That is to say, both Pd and Pt are inevitable factors that give Pt/Pd/C catalysts better activity and durability.

3.3. Single cell testing

Considering the activity and durability in the half cell testing, $Pt_1/Pd_2/C$ was selected to be evaluated under single cell conditions, which are more similar to the real operation conditions of vehicles. Meanwhile, 40% Pt/C (JM) catalyst was also be tested as a reference. The Pt loading for the cathode made by 40% Pt/C (JM) and $Pt_1/Pd_2/C$ was 0.29 and 0.16 mg_{Pt} cm^{-2} measured by ICP, respectively. The ADT protocol for potential cycling is usually used for the evaluation of catalyst durability to simulate the potential change during the operating conditions on vehicles. In our experiments, the cathode was cycled between 0.65 and 1.05 V (vs. DHE), since 0.65 V is close to the usual working point of fuel cells and 1.05 V is a little higher than the open circuit voltage in order to accelerate the degradation. Additionally, the scan rate was 100 mV s^{-1}, because it is reported that the faster scan rate will lead to faster degradation of catalysts [5].

The IR-corrected polarization and CV curves for the fuel cells with cathodes made by the two catalysts after different potential cycles were shown in Fig. 9. And the corresponding variations of ECSA and cell voltage at 600 mA cm^{-2} are presented in Fig. 10. For Pt/C catalysts after 40,000 potential cycles, the loss of ECSA is about 50% and the cell voltage at 600 mA cm^{-2} declines over 30 mV. The ECSA and performance loss can be mainly attributed to the Pt nanoparticles aggregation triggered by potential cycling. It is reported that potential cycling leads to the oxidation and dissolution of Pt. The dissolved Pt ions or complexes will re-deposit on the larger Pt nanoparticles (Ostwald ripening) or diffuse into the ionomer or membrane and be chemical reduced by the H_2 crossover from the anode [5,34].

Interestingly, we found that the performance of fuel cells with $Pt_1/Pd_2/C$ cathode was enhanced after potential cycling and the performance did not decline until 40,000 potential cycles. As shown in Fig. 10, after 40,000 cycles, the cell voltage at 600 mA cm^{-2} for fuel cell with $Pt_1/Pd_2/C$ cathode is increased by more than 70 mV. The loss of ECSA for $Pt_1/Pd_2/C$ cathode after 80,000 cycles was only about 30% which is much smaller than that of the Pt/C cathode, indicating better electrochemical durability for Pt/Pd/C catalysts under fuel cell working conditions. The Pt mass activity for the three catalysts before and after single-cell ADT is compared in Fig. 11. After potential cycling, the Pt mass activity for Pt/C is reduced, while that of Pt/Pd/C catalysts is considerably enhanced. Particularly, the Pt mass activity at 0.7 V of $Pt_1/Pd_2/C$ is about 4.5 times that of Pt/C after single-cell ADT.

In the half cell testing, it has been observed that the Pd will dissolve during potential cycling. In the single cell testing, we have also found the dissolution of Pd. As shown in Fig. 9 (d), the shape of H_{upd} region on the CV curves for $Pt_1/Pd_2/C$ cathode changed significantly after ADT, i.e., from arc to a more flat curve with distinct peaks. The arc curve can be attributed to the concurrent presence of metallic Pt and metallic Pd [32,35], while the flat curve with distinct peaks is the characteristic of pure Pt and the distinct peaks

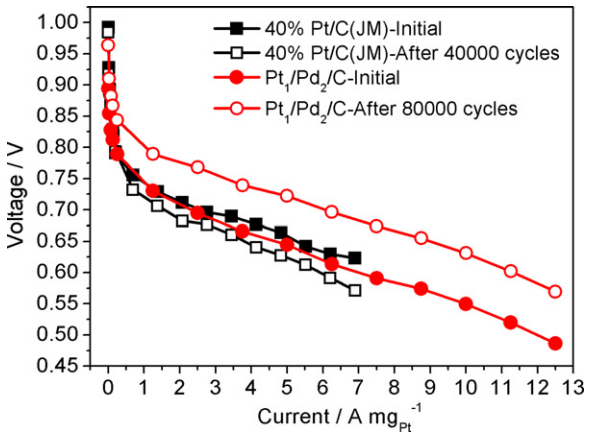

Fig. 11. IR-corrected polarization curves for the fuel cells with cathodes made by the 40% Pt/C (JM) and $Pt_1/Pd_2/C$ catalysts before and after single-cell ADT. Solid and open symbols represent polarization curves before and after single-cell ADT, respectively. The current is normalized to the Pt loading of the cathode.

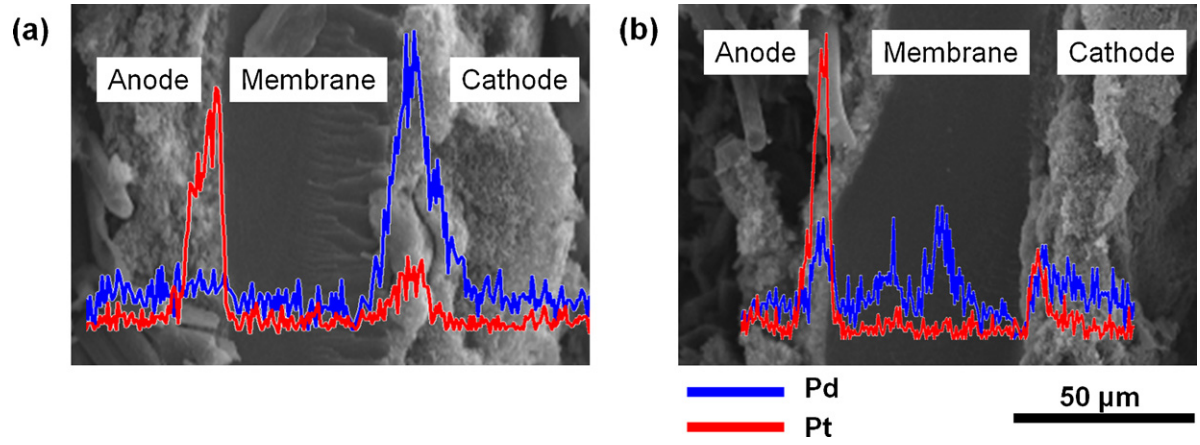

Fig. 12. SEM and elemental line profile of the cross-sectional MEAs with cathode made by $Pt_1/Pd_2/C$ before (a) and after (b) single-cell ADT.

come from the hydrogen desorption from Pt surfaces with different index [36]. The change of CV curve shape for $Pt_1/Pd_2/C$ after potential cycling illustrates the dissolution of Pd induced by the potential cycling.

In order to monitor the contribution of Pd element in MEA directly, the cross-sectional MEA with $Pt_1/Pd_2/C$ cathode before and after ADT was detected by SEM-EDX measurements (Fig. 12). In the pristine MEA, the Pd peak only appears in the cathode. However, in the aged MEA, the Pd peak in the cathode is remarkably weakened, and the Pd signal can be found in membrane and anode, confirming the dissolution of Pd from cathode catalysts. The dissolved Pd will diffuse into the membrane and anode, and then be reduced by the H_2 from anode. The above result further confirms the dissolution of Pd on the cathode during potential cycling.

As observed in the half cell testing, $Pt_1/Pd_2/C$ catalysts have presented enhanced durability due to the dissolution of Pd. Similarly, Pd dissolved from $Pt_1/Pd_2/C$ during single-cell ADT. Sasaki et al. [6] have found that the slow oxidation of Pd will impede excursions of the cathode potentials to high values, which will increase the stability of Pt by shifting positively its oxidation potential. That may explain the lower degradation rate of ECSA for $Pt_1/Pd_2/C$ than that of Pt/C. In addition, the degradation conditions of single-cell ADT is milder than that of half-cell ADT, so the dissolution of Pd and the corresponding structure transformation is delayed. As a result, we observed the improvement of the performance of the $Pt_1/Pd_2/C$ cathode in the first 40,000 potential cycles, which may reflect the structure transformation of $Pt_1/Pd_2/C$ catalysts. Thanks to the structure transformation, the Pt mass activity of $Pt_1/Pd_2/C$ catalysts after single-cell ADT is greatly higher than that of Pt/C, indicating that the activity of the pristine catalysts can be maintained or even enhanced in the actual dynamic loading conditions, that is, the durability of $Pt_1/Pd_2/C$ catalysts is better than that of the conventional Pt/C catalysts.

4. Conclusions

Pt modified Pd/C catalysts (Pt/Pd/C) with a $Pd_{core}@Pt_{shell}$ structure at Pt/Pd molar ratio of 1:4, 1:2 and 1:1 are synthesized by a chemical reduction method for ORR. The core–shell structure was proved by TEM, XRD and CV measurements. In the half cell testing, $Pt_1/Pd_4/C$ has the highest Pt mass activity for ORR, while $Pt_1/Pd_2/C$ and $Pt_1/Pd_1/C$ has much better durability than commercial Pt/C under potential cycling. After half-cell ADT, the $Pd_{core}@Pt_{shell}$ structure is converted to Pt-Pd alloy with Pt rich outer surface. This structure transformation is believed to enhance the ORR specific activity and hence result in the better durability of Pt/Pd/C catalysts. In the single cell testing, the loss of ECSA for $Pt_1/Pd_2/C$ cathode after 80,000 cycles was only 30% which is much smaller than that of the Pt/C cathode (50% loss after 40,000 cycles), indicating much better electrochemical durability for Pt/Pd/C catalysts under fuel cell working conditions. More interestingly, the polarization performance of Pt/Pd/C cathodes is improved after ADT, i.e., the Pt mass activity is increased by potential cycling, while the activity for Pt/C is decreased. It is particularly important and informative that at 0.7 V after ADT, the Pt mass activity of $Pt_1/Pd_2/C$ is about 4.5 times that of Pt/C. The improvement of Pt/Pd/C activity is believed to be associated with the dissolution of Pd core and the corresponding structure transformation. We believe that further optimization in the MEA manufacture could further enhance the performance of Pt/Pd/C cathode. Therefore, the Pt/Pd/C catalyst with high activity and durability is expected to be a promising low-Pt cathode electrocatalyst with potential application in PEMFCs.

Acknowledgements

This work was financially supported by the National High Technology Research and Development Program of China (Nos. 2011AA11A273, 2011AA050701) and the National Natural Science Foundations of China (Nos. 21076208, 20936008).

Appendix A. Supplementary data

Supplementary data associated with this article can be found, in the online version, at http://dx.doi.org/10.1016/j.apcatb.2012.11.029.

References

[1] Y. Wang, K.S. Chen, J. Mishler, S.C. Cho, X.C. Adroher, Applied Energy 88 (2011) 981.
[2] Y.H. Bing, H.S. Liu, L. Zhang, D. Ghosh, J.J. Zhang, Chemical Society Reviews 39 (2010) 2184.
[3] K. Lee, J.J. Zhang, H.J. Wang, D.P. Wilkinson, Journal of Applied Electrochemistry 36 (2006) 507.
[4] M.K. Debe, Journal of Power Sources 161 (2006) 1002.
[5] S. Chen, H.A. Gasteiger, K. Hayakawa, T. Tada, Y. Shao-Horn, Journal of the Electrochemical Society 157 (2010) A82.
[6] K. Sasaki, H. Naohara, Y. Cai, Y.M. Choi, P. Liu, M.B. Vukmirovic, J.X. Wang, R.R. Adzic, Angewandte Chemie-International Edition 49 (2010) 8602.
[7] V.R. Stamenkovic, B. Fowler, B.S. Mun, G.F. Wang, P.N. Ross, C.A. Lucas, N.M. Markovic, Science 315 (2007) 493.
[8] J.X. Wang, H. Inada, L.J. Wu, Y.M. Zhu, Y.M. Choi, P. Liu, W.P. Zhou, R.R. Adzic, Journal of the American Chemical Society 131 (2009) 17298.
[9] U.A. Paulus, A. Wokaun, G.G. Scherer, T.J. Schmidt, V. Stamenkovic, N.M. Markovic, P.N. Ross, Electrochimica Acta 47 (2002) 3787.
[10] H.A. Gasteiger, S.S. Kocha, B. Sompalli, F.T. Wagner, Applied Catalysis B: Environmental 56 (2005) 9.
[11] E. Antolini, Energy & Environmental Science 2 (2009) 915.

[12] J.L. Zhang, M.B. Vukmirovic, Y. Xu, M. Mavrikakis, R.R. Adzic, Angewandte Chemie-International Edition 44 (2005) 2132.
[13] K. Sasaki, J.X. Wang, H. Naohara, N. Marinkovic, K. More, H. Inada, R.R. Adzic, Electrochimica Acta 55 (2010) 2645.
[14] B. Lim, M.J. Jiang, P.H.C. Camargo, E.C. Cho, J. Tao, X.M. Lu, Y.M. Zhu, Y.A. Xia, Science 324 (2009) 1302.
[15] M. Jiang, B. Lim, J. Tao, P.H.C. Camargo, C. Ma, Y. Zhuc, Y. Xia, Nanoscale 2 (2010) 2406.
[16] N.V. Long, M. Ohtaki, M. Nogami, T.D. Hien, Colloid and Polymer Science 289 (2011) 1373.
[17] K. Gong, M.B. Vukmirovic, C. Ma, Y. Zhu, R.R. Adzic, Journal of Electroanalytical Chemistry 662 (2011) 213.
[18] I. Choi, S.H. Ahn, J.J. Kim, O.J. Kwon, Applied Catalysis B: Environmental 102 (2011) 608.
[19] F. Taufany, C.-J. Pan, J. Rick, H.-L. Chou, M.-C. Tsai, B.-J. Hwang, D.-G. Liu, J.-F. Lee, M.-T. Tang, Y.-C. Lee, C.-I. Chen, ACS Nano 5 (2011) 9370.
[20] L. Wang, Y. Yamauchi, Journal of the American Chemical Society 132 (2010) 13636.
[21] Z.M. Peng, H. Yang, Journal of the American Chemical Society 131 (2009) 7542.
[22] W. Wang, R.F. Wang, S. Ji, H.Q. Feng, H. Wang, Z.Q. Lei, Journal of Power Sources 195 (2010) 3498.
[23] C. Wang, D. van der Vliet, K.L. More, N.J. Zaluzec, S. Peng, S.H. Sun, H. Daimon, G.F. Wang, J. Greeley, J. Pearson, A.P. Paulikas, G. Karapetrov, D. Strmcnik, N.M. Markovic, V.R. Stamenkovic, Nano Letters 11 (2011) 919.
[24] S. Koh, P. Strasser, Journal of the American Chemical Society 129 (2007) 12624.
[25] C. Wang, G.F. Wang, D. van der Vliet, K.C. Chang, N.M. Markovic, V.R. Stamenkovic, Physical Chemistry Chemical Physics 12 (2010) 6933.
[26] I. Takahashi, S.S. Kocha, Journal of Power Sources 195 (2010) 6312.
[27] J.X. Wang, C. Ma, Y. Choi, D. Su, Y. Zhu, P. Liu, R. Si, M.B. Vukmirovic, Y. Zhang, R.R. Adzic, Journal of the American Chemical Society 133 (2011) 13551.
[28] C. Wang, H. Daimon, T. Onodera, T. Koda, S. Sun, Angewandte Chemie-International Edition 47 (2008) 3588.
[29] J.-H. Jang, C. Pak, Y.-U. Kwon, Journal of Power Sources 201 (2012) 179.
[30] X.T. Zhang, H. Wang, J.L. Key, V. Linkov, S. Ji, X.L. Wang, Z.Q. Lei, R.F. Wang, Journal of the Electrochemical Society 159 (2012) B270.
[31] Y.N. Wu, S.J. Liao, Z.X. Liang, L.J. Yang, R.F. Wang, Journal of Power Sources 194 (2009) 805.
[32] J.H. Yang, W.J. Zhou, C.H. Cheng, J.Y. Lee, Z.L. Liu, ACS Applied Materials & Interfaces 2 (2010) 119.
[33] W. He, H. Jiang, Y. Zhou, S. Yang, X. Xue, Z. Zou, X. Zhang, D.L. Akins, H. Yang, Carbon 50 (2012) 265.
[34] P.J. Ferreira, G.J. la O, Y. Shao-Horn, D. Morgan, R. Makharia, S. Kocha, H.A. Gasteiger, Journal of the Electrochemical Society 152 (2005) A2256.
[35] D.L. Wang, H.L. Xin, Y.C. Yu, H.S. Wang, E. Rus, D.A. Muller, H.D. Abruna, Journal of the American Chemical Society 132 (2010) 17664.
[36] C.M. Sanchez-Sanchez, J. Solla-Gullon, F.J. Vidal-Iglesias, A. Aldaz, V. Montiel, E. Herrero, Journal of the American Chemical Society 132 (2010) 5622.